Numerical Simulation Analysis of Turbulent Pulsation Drag Reduction at Different Intervals

Kun Ying Wang and Bo Hua Sun *

Posted Date: 22 July 2024

doi: 10.20944/preprints202407.1706.v1

Keywords: Turbulence; Pulsation; Large eddy simulation(LES); Drag reduction

Article

Numerical Simulation Analysis of Turbulent Pulsation Drag Reduction at Different Intervals

Kun Ying Wang [1,2,3] and Bo Hua SUN [2,3,*]

[1] School of Architectural Science and Equipment Engineering, Xian University of Architecture and Technology, Xian 710055, China
[2] Institute of Mechanics and Technology, Xian University of Architecture and Technology, Xian 710055, China
[3] Beijing Institute of Nanoenergy and Nanosystems, Chinese Academy of Sciences, Beijing 101400, China
* Correspondence: sunbohua@binn.cas.cn

Abstract: The shear stress generated by wall turbulence is the main cause of wall friction resistance in turbulent flow through pipes. This paper investigates the impact of inserting rest periods (regions of constant Reynolds number) within the pulsating operating cycle of velocity on the fully turbulent flow at large time-averaged Reynolds numbers, using the Large Eddy Simulation (LES) method. The study aims to explore the effect of increasing rest periods within pulsations on drag resistance. The dimensionless shear stress and drag reduction rates during different time periods of rest were analyzed. Numerical simulation results indicate that the pulsating velocity operation mode does not necessarily lead to drag reduction; it may even result in increased resistance. Inserting rest periods within the pulsation cycle can achieve drag reduction effects, with the maximum drag reduction rate reaching 21.8%. Comparisons with experimental data and Direct Numerical Simulation (DNS) from the literature validate the feasibility of using the LES method for pipe pulsating operation modes.

Keywords: turbulence; pulsation; large eddy simulation (LES); drag reduction

1. Introduction

In today's world, changes are taking place rapidly, and the pace of development is accelerating, leading to an increasing demand for energy. Therefore, how to make full use of energy, develop new energy sources, and save energy has become an urgent issue that needs to be addressed. This issue has also drawn widespread attention from scholars and researchers. However, even with the development of new energy sources, energy is not inexhaustible. Reducing resistance is one of the important ways to save energy consumption.

Fluid resistance comes in several forms, with the most fundamental being pressure resistance and frictional resistance. [1]. In recent years, the reduction of friction drag in turbulent wall flows has garnered increasing attention due to the recognition of high energy consumption and the need to reduce the emission of pollutants into the atmosphere [2] . During the operation of various transportation vehicles, friction drag accounts for a significant proportion of the total resistance. For instance, in conventional transport aircraft and waterborne vessels, surface friction accounts for about 50% of the total resistance; for submarines operating underwater, this proportion can reach 70%; and in long-distance pipeline transportation, the power of pump stations is almost entirely used to overcome the work done by surface friction resistance. Flow through pipelines and hydraulic networks is typically turbulent, and the friction losses encountered in these flows account for approximately 10% of global electricity consumption. Turbulence can lead to a significant increase in resistance [3]. Therefore, the study of turbulence drag reduction is of great significance. In practical applications, the flow through pipelines and channels is the most common method of transporting fluids, and it also exists in many natural systems. In both natural and industrial processes, turbulence can have adverse or even detrimental effects, hence methods to suppress the accompanying unstable velocity and pressure fluctuations have significant practical importance [4]. How to reduce the resistance in pipeline transportation processes, increase pipeline throughput, thereby reducing energy consumption and saving costs, is a challenge that numerous engineers and researchers have been working hard to solve through extensive research over the years. This is especially true for long-distance oil, gas, and

 doi:10.20944/preprints202407.1706.v1

water pipelines, as their diameters and through puts are quite large. If their frictional resistance can be effectively reduced, the energy saved would be substantial, and it would actively promote global energy conservation, emission reduction, and environmental protection. Hence, research on turbulent drag reduction in circular pipes holds significant practical importance.

Current drag reduction methods primarily include riblet treatments, polymer additives, compliant wall techniques, microbubble methods, biomimetic drag reduction, wall vibration methods, as well as novel techniques such as wall suction/blowing, spanwise periodic wall vibration, active turbulence control, traveling wave drag reduction, air curtain drag reduction, and supercavitation drag reduction. Some of these methods have been widely applied, while others are still in need of further research due to limited theory and investigation. Turbulence is ubiquitous in nature and applications, characterized by high friction levels and significant pumping costs, leading scholars to continuously develop methods to control it. However, despite substantial efforts, no universally applicable solution has been found to date.

Controlling wall turbulence to reduce wall shear stress is an important topic in modern fluid mechanics [5]. Numerous strategies for turbulence control have been proposed to decrease resistance in shear flows [2,4,6–12]. Quadrio et al. experimentally assessed the drag reduction capabilities of an active open-loop technique in turbulent wall-bounded flows [7]. Moarref et al. investigated small-amplitude blowing and suction confined to the wall and demonstrated that properly designed downstream traveling waves (DTWs) can significantly reduce the receptivity of three-dimensional perturbations, including streamwise streaks and Tollmien-Schlichting waves [9]. Hof generated periodic turbulent puffs by introducing a small disturbance at the pipe inlet at Re = 2000, resulting in an intermittent flow. Experiments and numerical simulations indicate good drag reduction effects, and the energy gained by eliminating turbulence is about five times the cost [4]. Rathnasingham et al. conducted experimental studies on active control of the near-wall region of turbulent boundary layers using linear active control methods [10]. Scarsell and Hof proposed another method for controlling turbulence, which reduces drag through unsteady pulsating actuation, particularly simulating the cardiac cycle and extending this method to large Reynolds numbers [13]. Scarsell et al. studied the impact of pulsating velocity patterns on drag reduction in circular pipes using DNS methods and found that the maximum drag reduction rate can reach 27%. Pulsating actuation for drag reduction, in addition to being applied in the field of cardiovascular waveforms, can also be widely used in engineering applications [14], including biological flows such as pulmonary ventilation [15] and hemodynamics [16], sediment transport in submarine and coastal flows [17], and reciprocating flows in internal combustion engines [18]. In engineering, large-scale customized syringe pumps [13] or valves with controllable flow rates can be used to precisely control the flow to produce velocity with periodic fluctuations. There are currently numerous simulations and experimental studies on pulsating flows, with most simulations using Direct Numerical Simulation (DNS) methods. Scotti et al. used Computational Fluid Dynamics (CFD) to predict unsteady turbulence, not only validating the effectiveness of using Large Eddy Simulation (LES) methods in Fluent to study such unsteady flows but also comparing the simulation results of DNS direct numerical simulation, LES large eddy simulation methods in Fluent [19], and $k-\omega$ and $k-\varepsilon$ two-equation turbulence models [20],finding that the $k-\varepsilon$ two-equation turbulence model used in Fluent has higher accuracy in some aspects compared to the $k-\omega$ turbulence model.

Direct Numerical Simulation (DNS) of turbulence involves solving the complete Navier-Stokes equations to compute the time evolution of all instantaneous flow quantities in the flow field, including pulsations. Statistical analysis of the sample flow fields is then performed to obtain the mean characteristics of turbulence. This method is known as Direct Numerical Simulation of turbulence. To directly simulate turbulence, on one hand, the computational domain must be large enough to encompass the motion of the largest eddies, and on the other hand, the computational grid must be fine enough to resolve the motion of the smallest eddies. Therefore, DNS requires a significant amount of computational cost and resources [21]. Large Eddy Simulation (LES) is a compromise numerical

 doi:10.20944/preprints202407.1706.v1

simulation method that lies between DNS and Reynolds-Averaged Navier-Stokes (RANS). It uses spatial filtering techniques to separate different eddies, solving only for the large-scale eddies that play a major role in pressure fluctuations and filtering out the smaller eddies. Compared to DNS, LES reduces the demand for computational resources, and compared to RANS, LES can obtain more information about fluctuations [22].

Building on the research by Scarsell et al [13], this paper employs the large eddy simulation (LES) approach in the commercial software Fluent to investigate the impact of different steady-phase patterns of pulsatile flow on turbulent drag reduction in circular pipes. Scarsell employed Direct Numerical Simulation (DNS), which requires substantial computational resources. Therefore, this paper opts for the LES numerical simulation method. By using numerical methods, we will present the dimensionless shear stress in circular pipes driven by the same velocity pulsation curve function as found in the literature and compare it with existing experimental data to verify the reliability of the numerical calculation method.Subsequently, while maintaining the minimum and maximum Reynolds numbers of the velocity pulsation function and the total duration of the acceleration and deceleration phases, we will alter the stationary phases of the pulsation function. This will allow us to investigate the drag reduction in circular pipes driven by different stationary phases of the velocity pulsation function and compare it with the drag reduction in quasi-steady-state conditions. The optimal stationary phase of the velocity pulsation function that drives the circular pipe will be identified.

2. Numerical Method

2.1. Geometric Model and Boundary Conditions

A cylindrical pipe with a diameter $D = 30mm$ and a length $L = 7m$is modeled using Fluent for three-dimensional, unsteady simulations. The simulation starts at the pipe inlet and includes a development length of $60D$ to ensure fully developed flow conditions before measurements commence. The pressure drop Δp is measured over a length of $L = 120D$ within the pipe. the boundary conditions of the pipe are set up as velocity inlet, pressure outlet, the incoming flow along the negative direction of the z-axis, and the cylindrical surface is an adiabatic non-slip wall as shown in Figure 1.

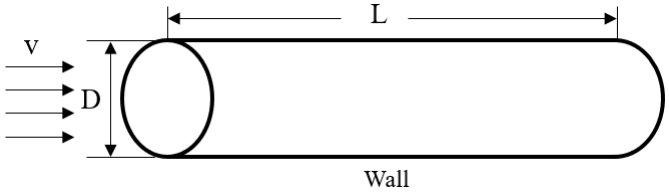

Figure 1. Geometric model and boundary conditions

2.2. Computational Conditions and Mesh

The cylindrical pipe model is discretized using a structured mesh generated by ICEM, as shown in Figure 2 for Large Eddy Simulation (LES). The mesh counts for the configurations in Figure 2(a), (b) and (c) are 70W, 143W and 200W, respectively. The mesh is refined at the pipe wall to ensure accurate resolution of the boundary layer, To maintain a non-dimensional wall distance $y^+ = 1$, the height of the first layer of mesh near the wall y is set to $1 \times 10^{-4}m$, the growth ratio of the mesh in the normal direction near the wall is controlled within 1.1 to ensure mesh quality and resolution in the near-wall region.

$$y^+ = \frac{uy}{\nu} \tag{1}$$

Where u is the near-wall friction velocity ν is the kinematic viscosity of the fluid.

 doi:10.20944/preprints202407.1706.v1

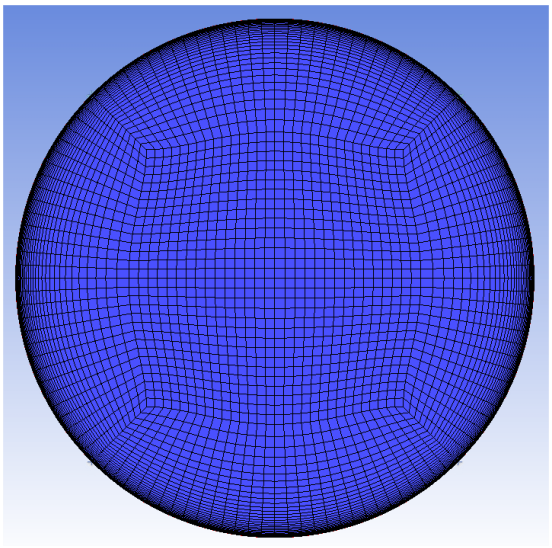

(a)Coarse grid

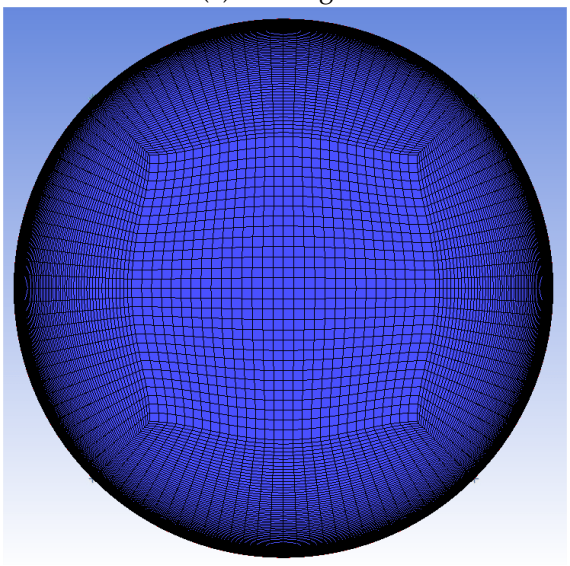

(b)Medium grid

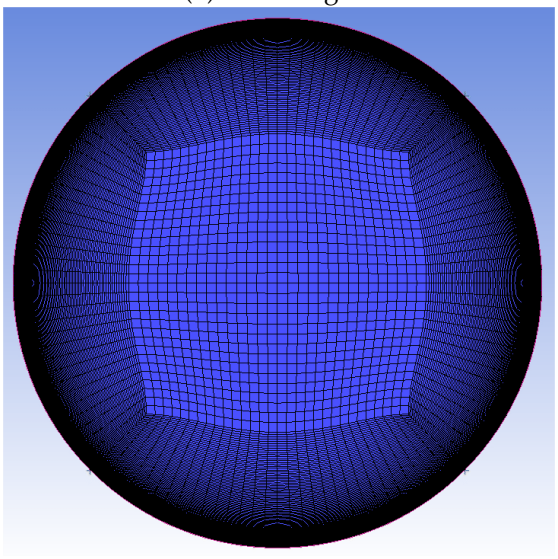

(c)Fine grid

Figure 2. Structured mesh illustration

 doi:10.20944/preprints202407.1706.v1

2.3. Large Eddy Simulation (LES) Control Equations

In this paper, a three-dimensional, unsteady, incompressible Large Eddy Simulation is performed to calculate the pressure drop Δp across a cylindrical pipe with a length of $L = 120D$ using ANSYS Fluent software. The simulation uses a pressure-based coupled solver, with the pressure-velocity coupling equations handled by the SIMPLE algorithm. Spatial discretization for both the pressure and momentum terms is implemented using a second-order differencing scheme.

In this study, the working conditions are illustrated in Figure 3. The medium inside the pipe is water, which is assumed to be incompressible, with temperature changes being negligible. The energy equation is not considered, only the continuity and momentum equations are taken into account. The fundamental idea of large eddy simulation is to filter the N-S equations, performing direct numerical simulation of eddies larger than the grid scale, while small-scale eddies are modeled using an appropriate subgrid-scale model. The governing equation is as follows :

$$\frac{\partial \widetilde{u_i}}{\partial x_i} = 0 \tag{2}$$

$$\frac{\partial \widetilde{u_i}}{\partial t} + \widetilde{u}_j \frac{\partial \widetilde{u_i}}{\partial x_j} = -\frac{1}{\rho}\frac{\partial \widetilde{p}}{\partial x_i} + \nu \frac{\partial}{\partial x_j}\left(\frac{\partial \widetilde{u_i}}{\partial x_j}\right) + \frac{\partial T_{ij}}{\partial x_j} \tag{3}$$

where ρ - fluid density; $\widetilde{p}$ - filtered pressure; $\widetilde{u_i}$ - filtered velocity component in the x_i direction ; T_{ij}- subgrid-scale stress tensor [23].

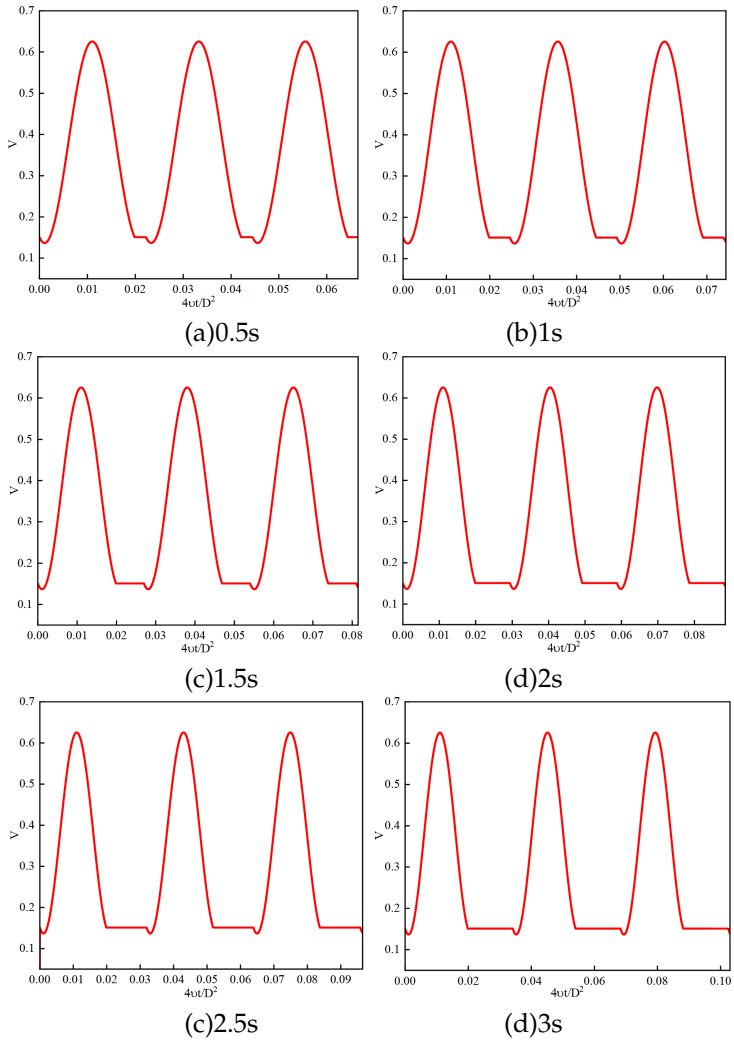

Figure 3. *Cont.*

Preprints.org (www.preprints.org) | NOT PEER-REVIEWED | Posted: 22 July 2024 doi:10.20944/preprints202407.1706.v1

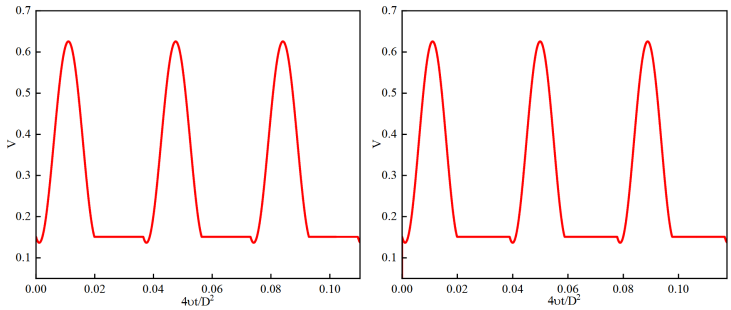

(c)3.5s (d)4s

Figure 3. Research working conditions curve

In this paper, the working conditions studied are shown in Figure 3. (a)∼(h) in Figure 3 present curve functions with additional intermittent periods of t=0.5s, 1s, 1.5s, 2s, 2.535s, 3s, 3.5s and 4s, respectively. These are based on a velocity function at the pipe inlet $v = 0.38117 + 0.24438\sin[\pi(t - 1.27226)/2.08921]$ with a period T is 4.17842s, amplitude of 0.24438, and intercept of 0.38117. The purpose is to investigate the impact of different resting phases within the velocity function at the inlet on the drag reduction rate in the pipe. The function $v = 0.38117 + 0.24438\sin[\pi(t - 1.27226)/2.08921]$ is the curve fitting function from Figure 2a in reference [13]. In Figure 3, v represents the velocity at the pipe inlet and $4\nu t/D^2$ denotes the dimensionless time.

3. Numerical Validation

Computational results from simulations using different mesh sizes are temporally averaged over five periods of the inlet velocity profile $v = 0.38117 + 0.24438\sin[\pi(t - 1.27226)/2.08921]$. These averaged results are compared with experimental and numerical findings from the literature, as summarized in Table 1. In the table, $\bar{\tau}^*$ represents the mean value over the five cyclic periods.

Table 1. Comparison of dimensionless shear stress

numerical example	$\bar{\tau}^*$	method
coarse grid	0.121203215	LES
medium Grid	0.121200056	LES
fine grid	0.121200048	LES
D.Scarsell	0.099652680	EXP
D.Scarsell	0.106277874	DNS

Where EXP denotes experiments, LES stands for Large Eddy Simulation, and DNS refers to Direct Numerical Simulation.

As observed from Table 1, when the mesh is coarse, the calculated values of $\bar{\tau}^*$ deviate from the experimental values by approximately 17.78%, and from the DNS results by about 12.31%. With further mesh refinement to a medium density and beyond, the calculated values of $\bar{\tau}^*$ exhibit minimal variation. Taking into account computational time, resources, and accuracy, this study selects a medium mesh density as the baseline for calculations. Subsequent assessments of drag reduction rates are referenced against the results obtained from the medium mesh density.

The dimensionless wall shear stress $\bar{\tau}^*$, as well as the formulas for drag reduction rate and quasi-steady values, are as follows:

$$\frac{\rho d U_m}{dt} = -\frac{\Delta p}{L} - \frac{4\tau_\omega}{D} \tag{4}$$

$$\tau^* = 2\tau_\omega/(\rho U_{min}^2) \tag{5}$$

 doi:10.20944/preprints202407.1706.v1

$$R = \frac{\tau^*_{steady} - \bar{\tau}^*}{\tau^*_{steady}} \tag{6}$$

$$\tau^*_{qs}(t) = 0.079 Re(t)^{-0.25} U_m(t)^2 / U^2_{min} \tag{7}$$

where U_m is the instantaneous bulk flow velocity; τ_ω is the wall shear stress; τ^* is the dimensionless wall shear stress; Δp is the pressure drop along the pipe over a length $L = 60D \sim 180D$ of the pipe (from the pipe inlet); τ^*_{steady} is the dimensionless constant flow wall shear stress derived from the Blasius friction factor correlation and normalized in a manner consistent with cyclic flows; R is the drag reduction rate; τ^*_{qs} is the quasi-steady reference condition, representing the anticipated wall shear stress when turbulent flow rapidly adapts to changes in Reynolds number, serving as a baseline for comparison [13].

Figure 4 presents a comparison of the calculated dimensionless wall shear stress from Large Eddy Simulation (LES) against experimental data and Direct Numerical Simulation (DNS) results as reported in reference [13], Figure 5 shows a comparison of the calculated dimensionless wall shear stress with quasi-steady values. As observed from the figures, while there are discrepancies between the LES results and both the experimental data and DNS outcomes, these deviations can be attributed to computational constraints on time and resources. The averaging period for LES results is significantly shorter compared to those from experiments and DNS. Additionally, the uncertainty in the exact form of the waveform function and the use of a fitted function different from that employed in the literature contribute to these discrepancies. Nonetheless, the fundamental trends and waveforms align well, and the LES results closely match the quasi-steady values τ^*_{qs}. This indicates that the numerical simulation methods used in this paper are reasonably accurate, with appropriate computational methodologies and settings ensuring the reliability of the results. Despite the limitations, the LES approach effectively captures the essential dynamics of the flow, validating the robustness of the adopted computational framework for the study at hand.

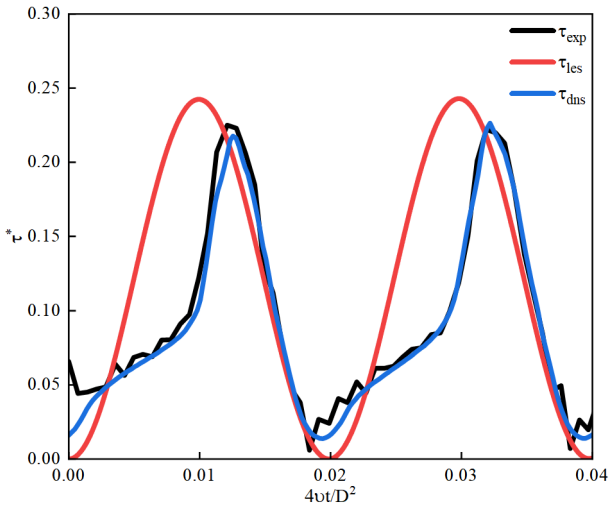

Figure 4. The comparsion of τ_{exp}, τ_{les}, τ_{dns}

Preprints.org (www.preprints.org) | NOT PEER-REVIEWED | Posted: 22 July 2024 doi:10.20944/preprints202407.1706.v1

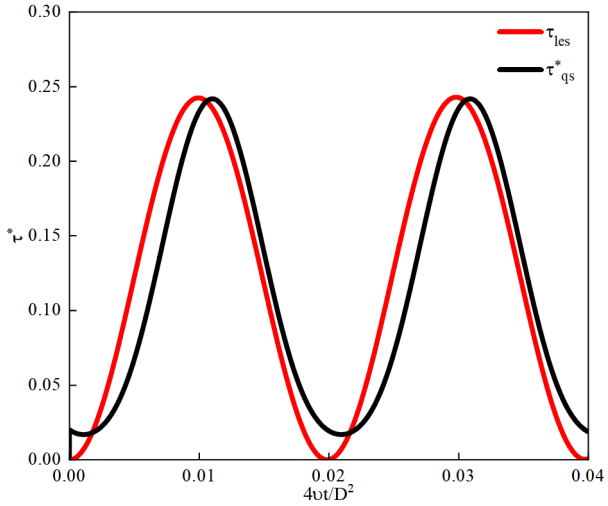

Figure 5. The comparsion of τ_{les} and τ^*_{qs}

4. Analysis and Discussion

4.1. Average Dynamic Pressure Drop

Figure 6 presents a comparison of the average dynamic pressure drop at the pipe inlet for various intermittent times. An intermittent time of T_r=0s corresponds to no rest period, with the velocity fluctuation function curve shown in Figure 7. For intermittent times of T_r=0.5s, 1s, 1.5s, 2s, 2.535s, 3s, 3.5s and 4s, Δp represents the average dynamic pressure drop over five cycles of the function. From Figure 6, As the intermittent time increases, Δp shows a decreasing trend, and when T_r=2.535s, Δp reaches its minimum value, compared with T_r=0s, Δp decreased by 38.66%. With further increases in the intermittent time T_r, Δp initially increases and then decreases. This indicates that a longer rest period is not always better; instead, there is an optimal value. An excessively long rest period can be counterproductive. The optimal rest period is approximately half the non-steady cycle time. When T_r=2.535s, the rest period is about half the cycle time $T = 4.17842$s of the function $v = 0.38117 + 0.24438\sin[\pi(t - 1.27226)/2.08921]$, which is consistent with the conclusions in the literature [13].

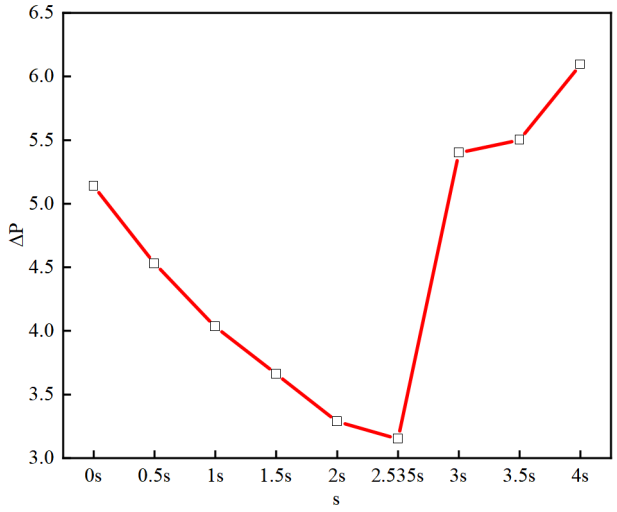

Figure 6. Comparison chart of average dynamic pressure drop at different intermittent times

Preprints.org (www.preprints.org) | NOT PEER-REVIEWED | Posted: 22 July 2024 doi:10.20944/preprints202407.1706.v1

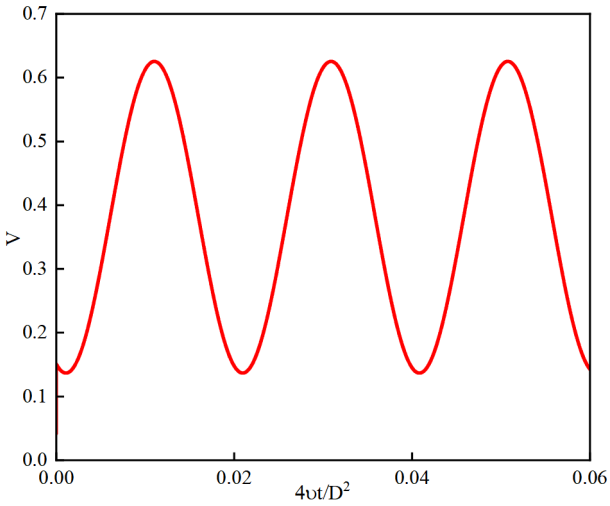

Figure 7. Velocity fluctuation function curve at T_r=0s

4.2. Analysis of Drag Reduction Rate

This section utilizes Equation (5) to analyze the drag reduction rate of the intermittent time function at the inlet. A comparison chart of the dimensionless wall shear stress $\bar{\tau}^*$ over five cycles for different intermittent time functions is depicted in Figure 8, where $\bar{\tau}^*$ represents the average value over five cyclic periods. Further analysis of the drag reduction rate through Equation (5) is illustrated in Figure 9. For this function, when the intermittent time is within the range of 0.5s∼2s, the pipe can achieve a drag reduction effect. When the intermittent time is within the range of 2s∼2.535s, the pipe experiences the best drag reduction effect, with the maximum drag reduction rate reaching 21.8%. However, when the intermittent time is within the range of 2.535s∼4s, not only is there no drag reduction effect, but there is also an increase in resistance. By analyzing Figures 8 and 9, it can be concluded that the intermittent time is not the longer the better; instead, there is an optimal value. When $t \times 4\nu/D^2 \approx 0 \sim 0.01$, adding a rest period in the middle of the pulsating velocity inlet is beneficial for drag reduction in the pipe; when $t \times 4\nu/D^2 \approx 0.01 \sim 0.012$, the drag reduction effect is optimal; when $t \times 4\nu/D^2 \approx 0.012 \sim 0.02$, adding a rest period in the middle of the pulsating velocity inlet not only fails to reduce drag but also leads to an increase in pipe resistance.

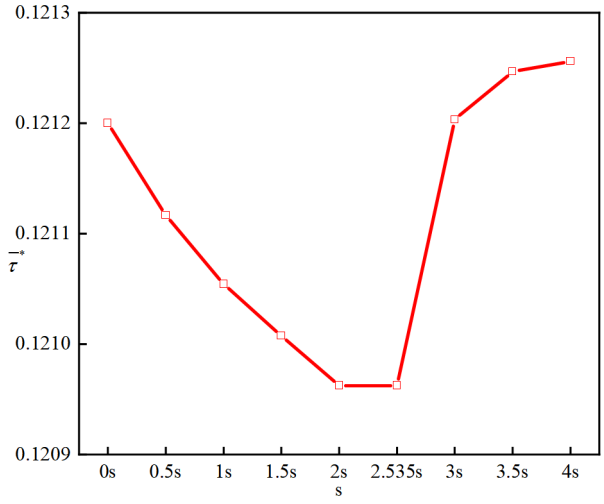

Figure 8. Plot of the variation of $\bar{\tau}^*$ for different intervals

 doi:10.20944/preprints202407.1706.v1

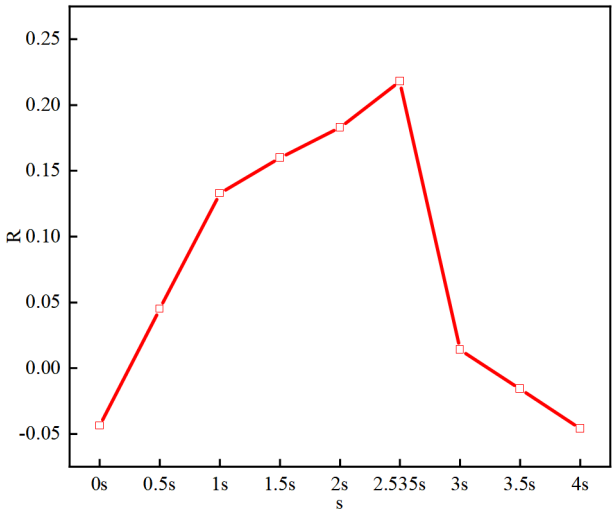

Figure 9. Drag reduction rates at different intermittent times

In daily life and practical applications, we take corresponding measures to increase or decrease resistance according to different needs. In moving machinery, to improve the operational efficiency of mechanical equipment and reduce energy loss, it is necessary to reduce frictional resistance. In fluid flow scenarios such as pipelines and rivers, reducing resistance can increase flow rates and decrease the energy required for pumping. In the design of transportation vehicles, reducing air resistance can improve fuel efficiency and increase speed. Athletes can reduce air or water resistance by wearing fitted clothing and improving techniques in sports like running and swimming. During downhill vehicle travel or emergency braking, increasing resistance can assist in slowing down; when driving on icy and snowy roads, equipping vehicles with anti-slip chains can increase friction with the ground, enhancing driving safety; in transportation means such as bicycles and cars, braking systems are used to increase frictional resistance to slow down or stop.

In summary, not all situations require drag reduction. In some cases, rather than reducing drag, it is actually necessary to increase resistance. This approach is tailored to the specific requirements of various applications, emphasizing the importance of a balanced and context-sensitive strategy in managing resistance forces.

4.3. Cloud Image Analysis

Figure 10 displays the pressure contour comparison at the pipe section L=60D, specifically at the start of the fifth cycle, for the original function and functions with different intermittent times. The analysis is conducted at the same curvature of the function curve. It can be observed from the figure that as the intermittent time increases, the pressure at the same cross-section gradually decreases. This indicates that an increased rest period provides favorable initial conditions and a lower level of turbulence for the subsequent acceleration phase, thereby achieving a drag reduction effect. However, the effectiveness of drag reduction should not be judged solely based on the pressure at one cross-section, but rather by the magnitude of the pressure drop. Although the instantaneous pressure at the same moment and cross-section decreases with the increase of intermittent time, the pressure drop at different cross-sections at the same moment first decreases and then increases as the intermittent time increases. This analysis underscores the importance of considering the pressure drop across multiple sections to comprehensively evaluate the impact of intermittent time on drag reduction in fluid flow systems.

 doi:10.20944/preprints202407.1706.v1

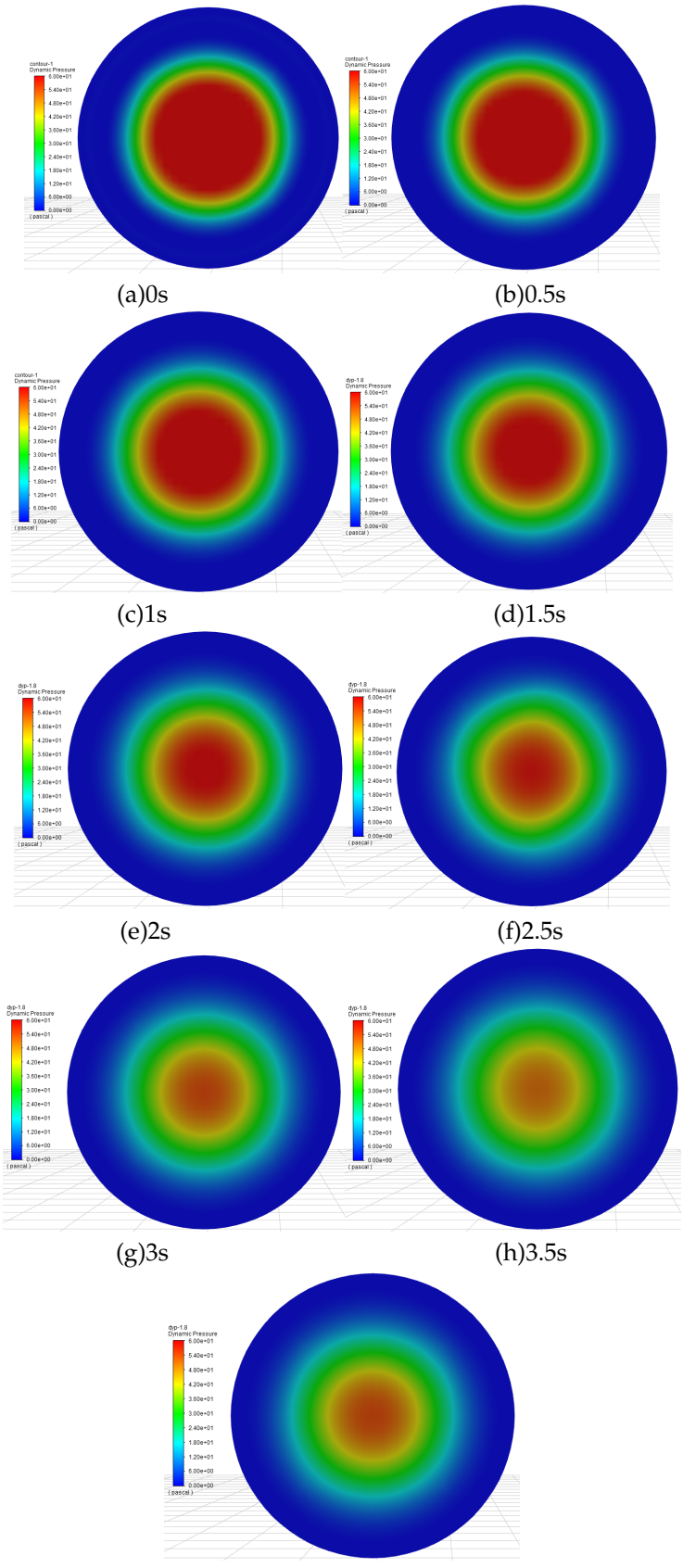

(a)0s (b)0.5s

(c)1s (d)1.5s

(e)2s (f)2.5s

(g)3s (h)3.5s

(h)4s

Figure 10. Pressure contour maps for different intermittent times

 doi:10.20944/preprints202407.1706.v1

5. Conclusion

In this study, the research subject is a circular pipe. Based on the pulsating velocity function at the entrance of the circular pipe, rest periods are added in the middle of the pulsation cycle. Within the same range of Reynolds numbers, the Large Eddy Simulation (LES) method is used to investigate the drag reduction capability of different rest periods for various pulsating velocity functions. The following conclusions are drawn:

(1)Using the Large Eddy Simulation (LES) method, this study compares the experimental results from existing literature with those from Direct Numerical Simulation (DNS), thereby validating the reliability of the numerical simulation approach.

(2)This study reaffirms that setting the velocity at the pipe inlet to a pulsating form does not necessarily result in drag reduction; it may, in fact, lead to an increase in resistance.

(3)Adding rest periods in the middle of the pulsating velocity function cycle at the pipe inlet effectively decouples the deceleration from the subsequent continuous acceleration phase. This provides favorable initial conditions for the next acceleration stage, thereby achieving a drag reduction effect.

Data Availability Statement: The data supporting the findings of this study are available from the corresponding author upon reasonable request.

Conflicts of Interest: The authors declare that there are no competing financial interests.

References

1. Dean, Brian, and Bharat Bhushan. "Shark-skin surfaces for fluid-drag reduction in turbulent flow: a review." Philosophical Transactions of the Royal Society A: Mathematical, Physical and Engineering Sciences 368.1929 (2010): 4775-4806.
2. Quadrio, Maurizio, Pierre Ricco, and Claudio Viotti. "Streamwise-travelling waves of spanwise wall velocity for turbulent drag reduction." Journal of Fluid Mechanics 627 (2009): 161-178.
3. Kühnen, Jakob, et al. "Destabilizing turbulence in pipe flow." Nature Physics 14.4 (2018): 386-390.
4. Hof, B, De Lozar, A, Avila, M., Tu, X, & Schneider, T. M. "Eliminating turbulence in spatially intermittent flows." science 327.5972 (2010): 1491-1494.
5. Ashill, P. R. "Flow Control: Passive, Active, and Reactive Flow Management M. Gad-el-Hak Cambridge University Press, The Edinburgh Building, Cambridge CB2 2RU, UK. 2000. 421pp." The Aeronautical Journal 105.1045 (2001): 150-150.
6. Du Y, Karniadakis G E. "Suppressing Wall Turbulence by Means of." science 288 (2000): 1230-1230.
7. Auteri, Franco, et al. "Experimental assessment of drag reduction by traveling waves in a turbulent pipe flow." Physics of Fluids,2010,22(11):115103.
8. Lieu, Binh K, Rashad Moarref, and Mihailo R. Jovanović. "Controlling the onset of turbulence by streamwise travelling waves. Part 2. Direct numerical simulation." Journal of Fluid Mechanics 663 (2010): 100-119.
9. Moarref, Rashad, and Mihailo R. Jovanović. "Controlling the onset of turbulence by streamwise travelling waves. Part 1. Receptivity analysis." Journal of fluid mechanics 663 (2010): 70-99.
10. Rathnasingham, Ruben, and Kenneth S. Breuer. "Active control of turbulent boundary layers." Journal of Fluid Mechanics 495 (2003): 209-233.
11. Willis, Ashley P, Yongyun Hwang, and Carlo Cossu. "Optimally amplified large-scale streaks and drag reduction in turbulent pipe flow." Physical Review E—Statistical, Nonlinear, and Soft Matter Physics 82.3 (2010): 036321.
12. Min, Taegee, et al. "Sustained sub-laminar drag in a fully developed channel flow." Journal of Fluid Mechanics 558 (2006): 309-318.
13. Scarselli, D, Lopez, J. M, Varshney, A, & Hof, B. "Turbulence suppression by cardiac-cycle-inspired driving of pipe flow." Nature 621.7977 (2023): 71-74.
14. Cheng, Z, et al. "Forcing frequency effects on turbulence dynamics in pulsatile pipe flow." International Journal of Heat and Fluid Flow 82 (2020): 108538.
15. Varghese, Sonu S, Steven H. Frankel, and Paul F. Fischer. "Direct numerical simulation of stenotic flows. Part 2. Pulsatile flow." Journal of Fluid Mechanics 582 (2007): 281-318.

 doi:10.20944/preprints202407.1706.v1

16. Xiao, Bin, and Yuwen Zhang. "Numerical simulation of pulsatile turbulent flow in tapering stenosed arteries." International journal of numerical methods for heat & fluid flow 19.5 (2009): 561-573.
17. Yan, B. H. "Analysis of laminar to turbulent transition of pulsating flow in ocean environment with energy gradient method." Annals of nuclear energy 38.12 (2011): 2779-2786.
18. Semlitsch, Bernhard, Yue Wang, and Mihai Mihăescu. "Flow effects due to pulsation in an internal combustion engine exhaust port." Energy conversion and management 86 (2014): 520-536.
19. Scotti, Alberto, and Ugo Piomelli. "Numerical simulation of pulsating turbulent channel flow." Physics of Fluids 13.5 (2001): 1367-1384.
20. Scotti, Alberto, and Ugo Piomelli. "Turbulence models in pulsating flows." AIAA journal 40.3 (2002): 537-544.
21. Wang X. "Investigation on the turbulence characteristics in the near field of round jet flow with DNS, RANS and LES. " ZJU(2010): 5-6.
22. SHI S K, HUANG X C, RAO Z Q, et al. "Study on force spectrum characteristics of a pump-jet under inflow turbulence. " Chinese Journal of Ship Research, 2022, 17(1): 1–C10.
23. Yu, Y. Q, A. Bergeron, and J. R. Licht. "Numerical simulation of involute-plate research reactor flow behavior using RANS, LES and DNS." Annals of Nuclear Energy 207 (2024): 110709.